Temperature and field hysteresis of the antiferromagnetic-to-ferromagnetic phase transition in epitaxial FeRh films

S. Maat, J.-U. Thiele, and Eric E. Fullerton
San Jose Research Center, Hitachi Global Storage Technologies, 650 Harry Road, San Jose, California 95120, USA
(Received 25 February 2005; revised manuscript received 11 October 2005; published 22 December 2005)

The temperature and field hysteresis of the magnetization in the first order antiferromagnetic to ferromagnetic phase transition in FeRh films grown onto *c*-axis sapphire and MgO (001) are investigated. The transition to the ferromagnetic state upon heating and antiferromagnetic state upon cooling is generally broad indicating a heterogeneous transition due to defects so that antiferromagnetic and ferromagnetic domains coexist during the transition. However, the nucleation of antiferromagnetic domains upon cooling is abrupt for FeRh on *c*-axis sapphire which is indicative of homogeneous nucleation and growth of antiferromagnetic domains. The transition is further broadened when measuring with fields applied out of plane of the sample due to internal demagnetization fields. Temperature dependent remanent magnetization measurements reveal that field induced magnetization changes are irreversible during heating, but reversible during cooling. The field dependence of the shift in transition temperature is qualitatively modeled with an Ising spin type model utilizing a mean field approach. From this calculation a shift of −10 K/T in transition temperature is determined in good agreement with the experimentally observed shift of −8 and −9 K/T for FeRh films grown onto MgO (001) and c-axis sapphire, respectively.

DOI: 10.1103/PhysRevB.72.214432 PACS number(s): 75.60.−d, 75.50.−y, 75.30.Kz

I. INTRODUCTION

In 1938 Fallot[1,2] discovered that bcc FeRh undergoes a first order phase transition from an antiferromagnetic (AF) to a ferromagnetic (*F*) phase upon heating from room temperature to above a transition temperature, T_{AF-F}, of approximately 370 K, with a temperature hysteresis of about 10 K between heating and cooling cycles. In subsequent studies it was further found that this transition is accompanied by a volume increase of 1%–2%,[3–5] a reduction in resistivity,[6–9] and a large change in entropy.[9–12] The Curie temperature of the ferromagnetic phase is about $T_{C\text{-}FeRh} \sim 670$ K.[3,7,10,13] Investigations of the two phases using Mössbauer spectroscopy[14] and neutron diffraction[15] revealed a collinear spin structure with moments of 3.2 μ_B per Fe and 0.9 μ_B per Rh atom for the *F* phase and a collinear spin structure with 3.3 μ_B per Fe atom and no magnetic moment on the Rh atom for the AF phase.The transition temperature can be tuned over a wide range by substitutional doping: the transition temperature increases with small additions of Ir or Pt, and decreases with small additions of Pd or Ni.[8,10,13] Furthermore, a shift to lower temperatures is also observed by applying an external magnetic field.[3,8] While other materials exhibiting similar first order AF to *F* phase transitions such as Ru-doped $CeFe_2$[16,17] are known, FeRh is unique in that the phase transition occurs around, and in the case of Ir-doped and Pt-doped FeRh significantly above, room temperature. Beyond the interest in the fundamental physics of the magnetism of these materials, this makes FeRh an interesting material for potential technological applications. For example, it was recently proposed to use exchange coupled FeRh/FePt bilayers for thermally assisted magnetic recording media.[5,18,19] In this scheme, at storage temperatures $T_S < T_{AF-F}$ the antiferromagnetic phase of FeRh helps stabilizing the magnetization of the hard FePt layer, while at write temperatures $T_{AF\text{-}F} < T_W < T_{C\text{-}FeRh}$ the additional moment of the ferromagnetic FeRh helps magnetization reversal of the high anisotropy FePt layer via an exchange spring mechanism. Moreover, in optical pump-probe measurements using femtosecond laser pulses it was demonstrated that the AF-*F* phase transition can be driven within a few ps,[20,21] allowing the switching from one phase to the other on time scales relevant for thermally assisted recording and microelectronics applications.

In the present manuscript we investigate the magnetization temperature hysteresis at fixed external applied magnetic field and the magnetization field hysteresis at fixed temperature of 110-nm-thick $Fe_{49}Rh_{51}$ films grown onto MgO (001) and Al_2O_3(0001) [*c*-axis sapphire].

II. EXPERIMENTAL PROCEDURES

The 110-nm-thick $Fe_{49}Rh_{51}$ films were deposited by sputtering from an FeRh alloy target at 2 mTorr Ar pressure onto single crystal MgO and sapphire substrates preheated to 300 °C. Both samples were deposited simultaneously, and no seed layers were used. After the deposition the samples were annealed *in situ* at 800 °C for about 30 min in order to obtain the chemically ordered bcc phase of FeRh. After cooling down the samples were capped with a 2 nm Pt layer to avoid oxidation.

The crystal structure and epitaxy were characterized by x-ray diffraction and the FeRh stoichiometry was determined by Rutherford backscattering. Magnetization measurements were performed in a vibrating sample magnetometer (VSM) in a temperature range from 298 to 473 K in fields up to 2 T, and in a superconducting quantum interference device (SQUID) magnetometer in a temperature range from 200 to 400 K in fields up to 5 T. Discrete temperature steps were used in the VSM, while a temperature sweep rate of 1 K/min was used for the SQUID measurements.

 ©2005 The American Physical Society

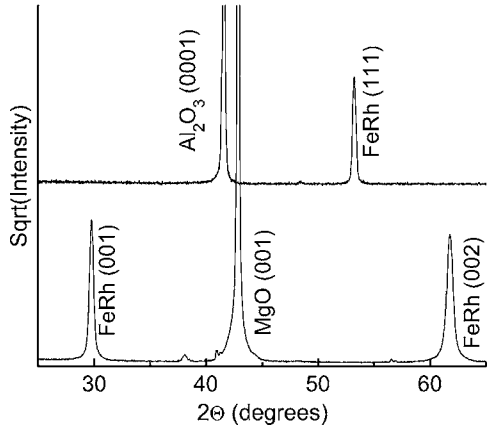

FIG. 1. Out-of-plane x-ray diffraction pattern for 110-nm-thick FeRh (001) on MgO (001) and FeRh (111) on Al_2O_3(0001) (*c*-axis sapphire). X-ray diffraction results are summarized in Table I.

III. X-RAY DIFFRACTION

The x-ray $\Theta-2\Theta$ scans shown in Fig. 1 reveal a FeRh (001) orientation on MgO (001) and a FeRh (111) orientation on *c*-axis sapphire. The full width at half maximum of the rocking curves of the FeRh peaks are 0.5° and 0.8° for FeRh on MgO and sapphire, respectively. The presence of the FeRh (001) confirms that the chemically ordered phase has been achieved. Table I summarizes the in-plane and out-of-plane lattice constants and strain parameters of the FeRh on MgO and FeRh on *c*-axis sapphire films measured at room temperature which corresponds to the lower volume AF phase for both films. The strain values are derived from the experimental lattice parameter of 2.988Å for bulk FeRh in the AF phase.[3]

While the FeRh on MgO film is slightly expanded out-of plane and compressed in-plane (tetragonal distortion) the FeRh on *c*-axis sapphire film is compressed out-of-plane and expanded in-plane (trigonal distortion) due to the larger lattice constant of the sapphire. The FeRh unit cell volume is about the same for both films. However, since the FeRh exhibits a larger lattice constant in the *F* phase than in the AF phase it can be expected that the *c*-axis sapphire tends to stabilize the *F* phase as it is easier to expand the crystalline lattice out of plane than in-plane as the temperature is increased.

IV. MAGNETIZATION DEPENDENCE ON TEMPERATURE AND MAGNETIC FIELD

According to the sample strain determined by x-ray diffraction the AF to *F* and *F* to AF transition temperatures are expected to be lower for FeRh grown onto *c*-axis sapphire than on MgO. This is indeed observed in temperature hysteresis loops measured for example in a 1 T external magnetic field applied in the plane of the sample as shown in Figs. 2(a) and 2(b) for the FeRh/MgO and FeRh/Al_2O_3 sample, respectively. The FeRh/Al_2O_3 sample transition temperature is ~30 K lower than that of FeRh/MgO. There are several distinct temperatures as indicated in Fig. 2(a): Upon heating ferromagnetic domains are nucleated at T_1 where a positive slope in the M vs T curve is observed. At T_2 the maximum magnetic moment for the heating cycle is reached and the sample is completely ferromagnetic. Consequently, for $T > T_2$ the magnetization follows a Curie-Weiss curve commonly observed in simple ferromagnetic materials.[10,18,22] Upon cooling the maximum magnetic moment for the cooling cycle is reached at T_3, and for $T < T_3$ ferromagnetic domains start to annihilate and are being replaced by AF domains. At T_4 the sample is almost completely AF and the moment is reduced to a small residual value. As can be seen in Fig. 2 the AF–*F* phase transitions are broad, extending over approximately 50 K. For a perfect sample the transition would be abrupt with $T_1=T_2>T_3=T_4$. However, due to residual crystalline imperfections and chemical disorder the first order transition is broadened[23] so that the nucleation of *F* domains upon heating at T_1 happens below the nucleation of AF domains at T_3 upon cooling. ($T_3>T_1$). This diffusiveness of the transition implies coexistence of the *F* and AF phase between T_1 and T_2 during heating and T_3 and T_4 during cooling. T_{AF-F} and T_{F-AF} are defined as the temperatures where half of the maximum moment in the fixed field measurement upon heating and cooling is reached, i.e., where half of the moments at T_2 and T_3 are reached, respectively. The magnetization of ~1120 emu/cm^3 at 400 K for FeRh on MgO and *c*-axis sapphire is consistent with measurements on bulk FeRh.[7,10]

Temperature hysteresis loops of the magnetization (M) in a constant in-plane field and the remanent magnetization (M_R) after applying an in-plane field of the FeRh/MgO sample were studied upon heating and cooling to investigate the reversibility of magnetization changes. For the fixed field

TABLE I. Lattice constant and strain parameters of FeRh in FeRh(001)/MgO(001) and FeRh(111)/Al_2O_3(0001) films measured by x-ray diffraction along different crystallographic directions of the film. Ψ is the polar angle between the scattering vector and the sample surface normal.

FeRh/MgO	FeRh/Sapphire	ψ (°)	(Å) FeRh/MgO	Strain (%) FeRh/MgO	(Å) FeRh/sapphire	Strain (%) FeRh/sapphire
(002)	(111)	0.0	2.9980	+0.33	2.9800	−0.27
	(110)	35.2			2.9854	−0.09
(011)		45.0	2.9890	+0.03		
	(200)	54.7			2.9901	+0.07
(020)	(1-10)	90.0	2.9750	−0.44	2.9950	+0.23

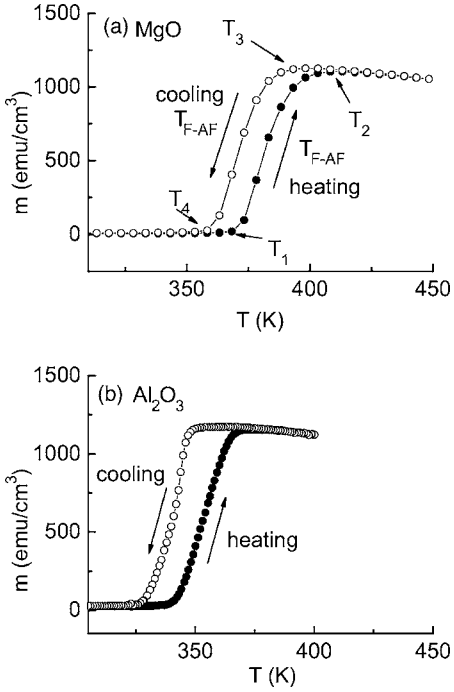

FIG. 2. Temperature hysteresis for the same 110-nm-thick FeRh films from Fig. 1 grown onto (a) MgO(001) and (b) Al_2O_3(0001). The temperatures T_1 and T_2 are defined in the heating cycle and T_3 and T_4 in the cooling cycle. The magnetic moment at T_{AF-F} is half the moment at T_2 and at T_{F-AF} half the moment at T_3.

magnetization measurement in the heating (cooling) cycle the temperature was increased (decreased) in a constant external field. For the M_R measurement in the heating (cooling) cycle the external field was removed upon reaching the target temperature, the remanent moment measured, the field reapplied and the temperature increased (decreased) to the next target temperature.

The magnetization curves (M-T) in a fixed field for the increasing and decreasing temperature are shown in Figs. 3(a) and 3(b), respectively, while the remanent magnetization curves (M_R-T) for increasing and decreasing temperature are shown in Figs. 3(c) and 3(d), respectively. As the external magnetic field is increased both T_1 (the temperature where ferromagnetic domains nucleate upon heating) and T_3 (the temperature where antiferromagnetic domains nucleate upon cooling) are decreased in the M-T curves. T_{AF-F} and T_{F-AF} are both decreased at the same rate of ~ -8 K/T, so that the width of the fixed field temperature hysteresis remains constant at ~ 11 K. This observation is consistent with bulk measurements where a shift of -8.3 K/T was observed.[3] Note that for fields above 2 T the entire temperature hysteresis is shifted below 400 K, enabling the measurement of T_{AF-F} and T_{F-AF} by SQUID magnetometry in external fields between 2 and 5 T. Since the magnetic field decreases the transition temperature the change in magnitude of the order parameter, i.e., the magnetization increases and hence a tricritical point where the first order phase transition becomes a second order phase transition should be absent in the H-T phase diagram.

The observation of a decreasing transition temperature with constant temperature hysteresis width in increasing external magnetic fields is similar to the behavior observed in Ru-doped $CeFe_2$.[16,17] However, in the Gd/Fe multilayer system which exhibits a first order ferrimagnetic to ferromagnetic phase transition a different behavior is observed: In this system the width of the hysteresis decreases with applied field and vanishes at some critical field giving rise to a spin-flop transition.[24] This point therefore could be identified as tricritical point for the Fe/Gd system above which the transition becomes second order.

We further found that for the remanent magnetization measurements only $T_{AF-F}(M_R)$ decreases with increasing field at about the same rate as T_{AF-F} for the fixed field magnetization measurement. In contrast $T_{F-AF}(M_R)$ is independent of the external field: As the external field is removed the field induced changes in the magnetization are irreversible upon heating, but reversible upon cooling. This indicates that applying an external field stabilizes the ferromagnetic phase and that the term superheating seems to be more appropriate than supercooling.

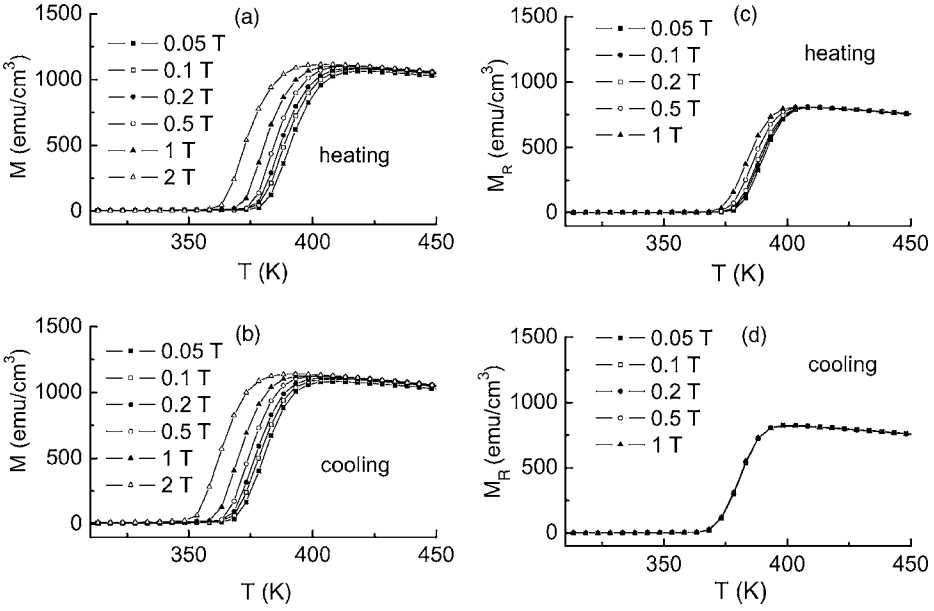

FIG. 3. Magnetization vs temperature hysteresis for heating (a) and cooling (b) in constant in-plane field, remanent magnetization (M_R) vs temperature hysteresis for heating (c) and cooling (d).

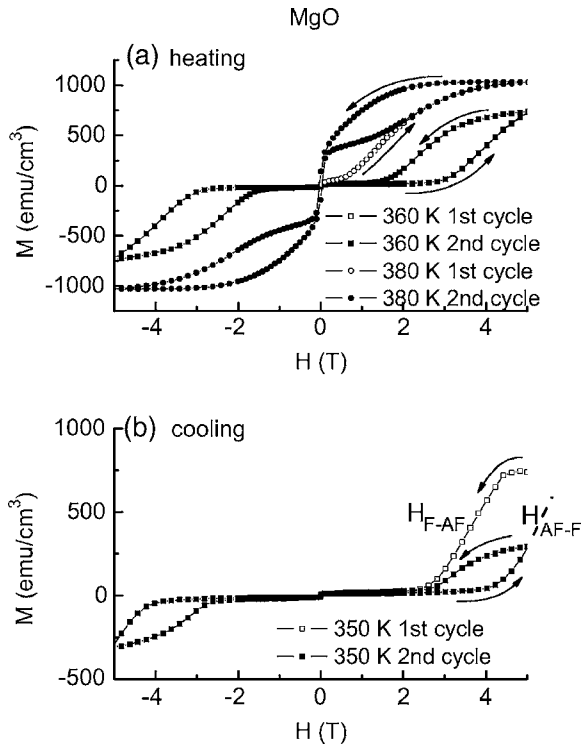

FIG. 4. (a) Field hysteresis loops for FeRh/MgO(001) upon heating taken at 360 and 380 K. The open symbols show the initial curve after warming the sample to the measurement temperature in zero field. (b) Field hysteresis loops measured at 350 K after cooling to 350 K in a 5 T field. The open symbols show the initial curve after cooling the sample to the measurement temperature.

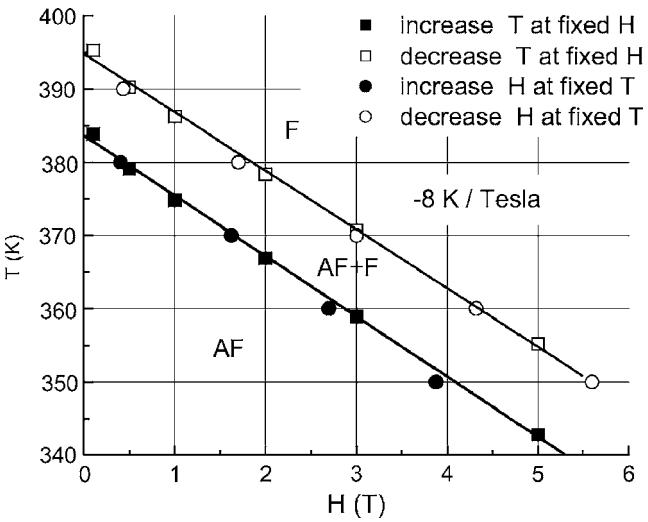

FIG. 5. *T-H* phase diagram for FeRh/MgO(001) as determined from magnetization vs temperature measurements in a fixed magnetic field and magnetization vs magnetic field measurements at a fixed temperature. The AF, AF+*F*, and *F* regions of the phase diagram are indicated in the figure.

To further investigate the reversibility between the *F* and AF phase field hysteresis loop measurements in the heating and cooling cycle were performed. For this the sample was heated in zero field from the AF phase to a temperature between T_1 and T_2 and an initial magnetization curve from 0 to 5 T followed by a full field hysteresis loop were recorded to check for irreversible changes in magnetization. To eliminate memory effects the field was removed and the temperature was reduced to 250 K (well below T_1 at zero field) after each field hysteresis loop measurement to completely transition into the AF phase before the sample was heated to the next higher temperature between T_1 and T_2 and recording another field hysteresis loop. Field hysteresis loops were taken between 350 and 400 K. The loops at 360 and 380 K are shown in Fig. 4(a). In these measurements it is observed that the field required to induce complete *F* order decreases with increasing temperature. Equivalent to the hysteresis in the temperature loop there is hysteresis in the positive and negative branch of the field loop as the sample transforms between the AF to the *F* phases. A 5 T field is not sufficient to fully induce *F* order between 350 and 370 K, but magnetization changes are reversible and the sample remains AF at zero field. Full *F* order is induced at 5 T between 380 and 400 K, however, at these temperatures some portion of the magnetization changes are irreversible and ferromagnetic order is maintained as the field is reduced from 5 to 0 T. All irreversible changes happen during the initial magnetization cycle, as indicated by the observation that the second field loop is closed. In these field hysteresis loops we define $H_{\mathrm{AF\text{-}F}}$ and $H_{\mathrm{F\text{-}AF}}$ as the fields where half of the saturation moment at a fixed temperature is reached upon increasing and decreasing the field, respectively. For simplicity, $H_{\mathrm{AF\text{-}F}}$ and $H_{\mathrm{F\text{-}AF}}$ are defined to be positive.

Field hysteresis loops were also recorded after cooling from 400 K in a 5 T field down to 340, 350, and 360 K. Here an initial magnetization loop from 5 to 0 T followed by a full field hysteresis loop were recorded. Again, to eliminate memory effects a 5 T field was applied and the temperature was increased to 400 K (well above T_2 at 5 T field) to completely transition into the *F* phase before the sample was cooled in 5 T to the next lower temperature between T_3 and T_4 and recording another field hysteresis loop. The loop taken at 350 K is shown in Fig. 4(b). Similar to the field loops taken upon heating hysteresis between the *F* and AF state is observed.

An *H* vs *T* phase diagram shown in Fig. 5 can be constructed by extracting the values of $H_{\mathrm{AF-F}}$ and $H_{\mathrm{F-AF}}$ from the field hysteresis loop measurements at fixed temperature and the values of $T_{\mathrm{AF-F}}$ and $T_{\mathrm{F-AF}}$ from the temperature hysteresis loop measurement in fixed field. Both datasets collapse onto two parallel lines. The data points for $H_{\mathrm{AF-F}}$ and $H_{\mathrm{F-AF}}$ at 350 and 360 K were determined from the field hysteresis loops taken upon cooling, the data points for 370, 380, and 390 K were determined from the field hysteresis loops taken upon heating. Data points for $H_{\mathrm{AF-F}}$ above 5 T are extrapolated as exemplified by $H_{\mathrm{AF-F}}$ (350 K) in Fig. 4(b) due to the 5 T field limitation of the SQUID. A linear function with slope $dT/dH=-8$ K/T gives a good fit to the data. However, using higher magnetic fields, McKinnon *et al.*[25]found that the AF$-F$ phase transition can be described by the empirical field-temperature relationship

$$\frac{H}{H_0} = 1 - \left(\frac{T}{T_0}\right)^2, \tag{1}$$

where H_0 and T_0 are composition dependent quantities describing the transition field at $T=0$ K and the transition temperature at $H=0$ T, respectively. With $dH/dT(T_0) = -1/8$ T/K and $T_0=(T_{AF-F}+T_{F-AF})/2=389$ K being the midpoint of the temperature hysteresis in the absence of an external field for FeRh/MgO, we obtain $H_0=24.3$ T, which is much larger than the magnetic fields than can be applied in the VSM or SQUID. Accordingly a linear temperature-field relationship for fields less than 5 T is a good approximation.

Using the measured slope of −8 K/T the entropy change ΔS associated with the magnetic phase transition can be calculated according to

$$\partial T/\partial H = -\frac{\Delta M}{\Delta S}, \tag{2}$$

where ΔM is the increase in magnetization once the transition into the F state is complete. For the observed value of $\Delta M=1120$ emu/cm^3 a value of $\Delta S=1.4\times10^6$ erg/cm^3 K $=140$ mJ/cm^3 is derived, which is in excellent agreement with the value of $\Delta S=14$ mJ/g K$=138$ mJ/cm^3 K obtained by Kouvel for bulk FeRh.[10] The latent heat absorbed by the FeRh system upon heating in fixed magnetic field can be calculated as

$$L = \int T(S)dS = \frac{\partial H}{\partial T}\int T(M)dM. \tag{3}$$

Using the temperature hysteresis data for heating at 0.5 T and integrating to the temperature (T_2) where the maximum magnetization value is reached a latent heat value of $L=5.2\times10^8$ erg/cm^3=52 J/cm^3 is calculated. For comparison the latent heat of melting ice is 334 J/cm^3 and of melting nitrogen is 25.5 J/cm^3. Since an applied magnetic field decreases the AF to F transition temperature about linearly the latent heat will decrease accordingly. The heat irreversibly lost after cycling through the transition can be calculated from the temperature hysteresis as

$$Q = \oint S(T)dT = \frac{\partial H}{\partial T}\oint M(T)dT \tag{4}$$

from which a value of $Q=1.7\times10^7$ erg/cm^3=1.7 J/cm^3 is obtained.

Investigations of the AF to F phase transition of the FeRh film grown onto c-axis sapphire similar to the previous discussed ones for the FeRh on MgO film were performed. In addition temperature hysteresis measurements were performed with the magnetic field applied perpendicular to the film plane. A heating and cooling cycle in 3 T in-plane and out-of-plane applied fields are shown in Fig. 6. This field overcomes the thin film demagnetization field of $4\pi M_S \sim 1.5$ T in the F state. Upon investigation of the in-plane temperature hysteresis loop it is apparent that the reversal for FeRh on sapphire is asymmetric as the heating and cooling behavior are distinct. Upon cooling a sharp initial creation of AF domains is observed, however, a similar sharp initial nucleation of F domains upon heating is absent. By cycling the temperature in fixed field and cycling the field at fixed temperature a phase diagram similar to that of Fig. 5 can be constructed from which a shift of the AF to F and F to AF transition temperature at a rate of −9 K/T is found. This rate is slightly higher than for FeRh/MgO, however according to Eq. (1) it is consisting with the lower AF-F transition temperature for FeRh/Al_2O_3. Similar to the FeRh on MgO sample the width and shape of the temperature hysteresis loops is independent of the applied field. In particular the sharp nucleation of the AF domains upon cooling is present at all magnetic fields up to 5 T.

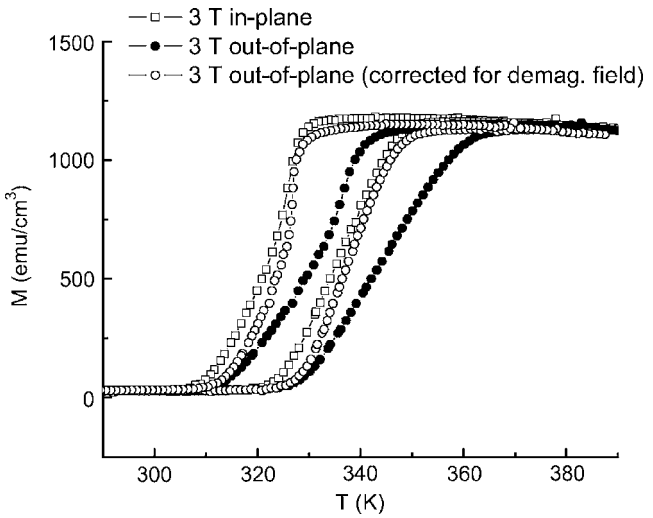

FIG. 6. In-plane and out-of-plane temperature hysteresis loops of FeRh on c-axis sapphire. The out-of-plane loop is broadened due to the FeRh demagnetization field. When corrected for the demagnetization field the loop exhibits a sharper transition, similar to the in-plane loop.

A comparison of the in-plane and out-of plane temperature hysteresis loops measured in a 3 T field shows that when the field is applied perpendicular to the film the transition is broadened and the nucleation of F domains is shifted to higher temperature. This arises from the self demagnetization field encountered when the magnetization is perpendicular to the film which tends to oppose the formation of the F phase. Using a mean field approach neglecting the effect of domains the demagnetization field can be corrected for by shifting the temperature by

$$\Delta T = dT/dH 4\pi M(T). \tag{5}$$

The perpendicular loop corrected for $dT/dH=-9$ K/T and $M_S=1250$ emu/cm^3 is included in Fig. 6. The transition width after correction becomes similar to the in-plane case and complete transition into the F phase upon heating and nucleation of AF domains upon cooling now occurs at about the same temperature as for the in-plane case. However, some deviation in particular in the lower part of the loop can be expected since the mean field approach neglects the effect of locally higher demagnetization fields in domains than calculated from the average magnetization.

In-plane field hysteresis loops for the FeRh/Al_2O_3 sample (similar to those for FeRh/MgO sample) were recorded be-

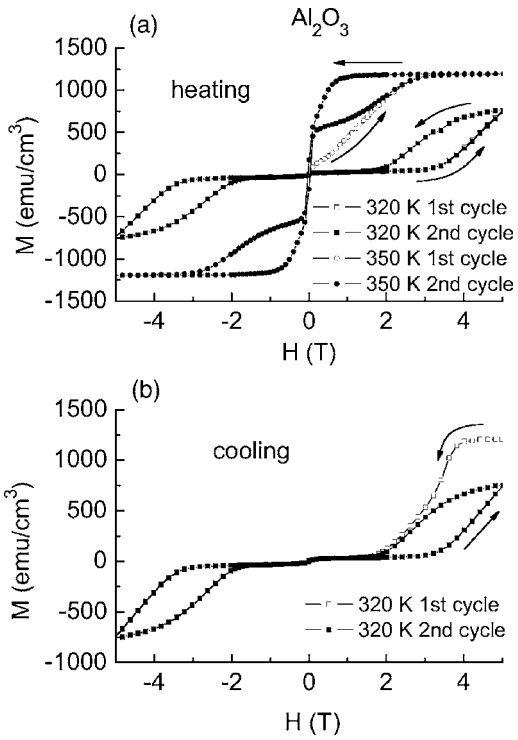

FIG. 7. Field hysteresis loops for FeRh/Al_2O_3(0001) upon heating taken at 320 and 350 K (a) and field hysteresis loop upon cooling taken at 320 K (b).

tween 320 and 360 K for the heating cycle and between 340 and 320 K for the cooling cycle. The loops at 320 and 350 K for the heating cycle and at 320 K for the cooling cycle are shown in Figs. 7(a) and 7(b), respectively. Again the field required to saturate the sample decreases with increasing temperature. A 5 T field is not sufficient to fully induce *F* order between 320 and 330 K, but magnetization changes are reversible and the sample remains AF at zero field. Full *F* order is obtained at 5 T between 340 and 360 K, however, some portion of the magnetization changes are irreversible and spontaneous magnetization develops as the field is reduced from 5 to 0 T. Remarkably the sharp nucleation of AF domains can also be observed in the field hysteresis data upon cooling, further emphasizing the symmetry between temperature and field hysteresis.

V. NUCLEATION KINETICS

It is interesting to investigate the magnetization change upon temperature cycling (dM/dT vs T) and upon field cycling (dM/dH vs H) in more detail to obtain insight into the cause of thermal smearing and transition kinetics. Figures 8(a) and 8(b) show the data for cycling the temperature in a field of 5 T for FeRh/MgO and cycling the magnetic field after heating from the AF phase to a temperature of 370 K, respectively. Figures 8(c) and 8(d) show the data for cycling the temperature in a field of 1 T and for cycling the magnetic field after heating from the AF phase to a temperature of 340 K, respectively, for FeRh/Al_2O_3.

By inspection of these curves, in particular for the FeRh/Al_2O_3 sample it is apparent that the magnetization

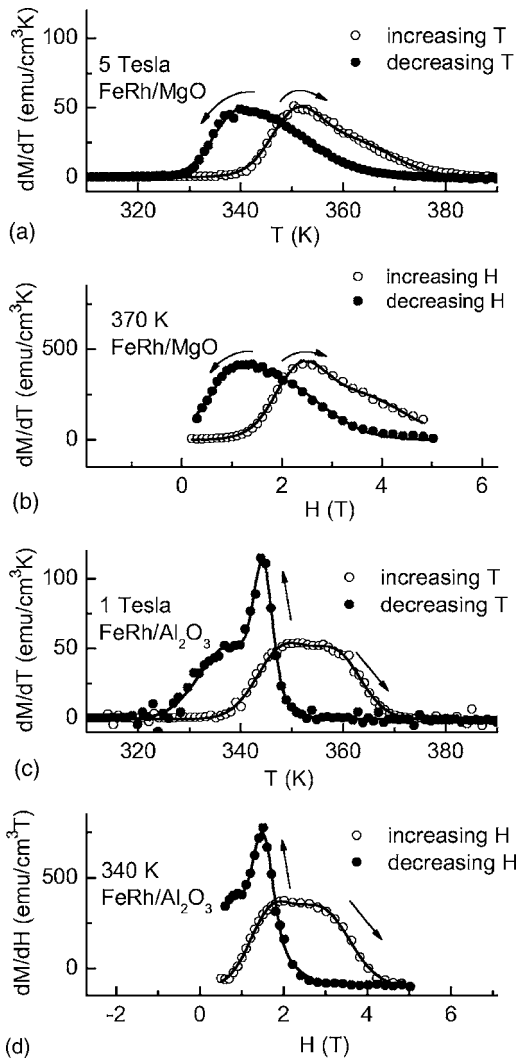

FIG. 8. Rate of *F* and AF domain nucleation and propagation for FeRh/MgO (001) upon (a) increasing and decreasing temperature (dM/dT) at 5 T and (b) increasing and decreasing field at 370 K. Rate of *F* and AF domain nucleation and propagation for FeRh/Al_2O_3(0001) (b) upon increasing and decreasing temperature (dM/dT) at 1 T and (d) and increasing and decreasing field (dM/dH) at 340 K. Temperatures for maximum *F* and AF nucleation and propagation rate can be identified. The AF nucleation peak is sharp indicating homogeneous transition from the *F* to the AF phase.

change with temperature, dM/dT, and the magnetization change with external field, dM/dH, can be fit by superposing two Gauss functions

$$dM/dT = (dM/dT)_1 \exp(z_1^2) + (dM/dT)_2 \exp(z_2^2), \quad (6)$$

where

$$z_i = (T - T_i)/\Delta T_i \quad (7)$$

and

$$dM/dH = (dM/dH)_1 \exp(z_1^2) + (dM/dH)_2 \exp(z_2^2), \quad (8)$$

where

TABLE II. Fitting parameters used to describe the nucleation and growth process of F and AF domains of FeRh on c-axis sapphire upon heating and cooling at 1 T and increasing and decreasing field after heating to 340 K. The fits are shown in Figs. 8(b) and 8(c).

Cycle T	$(dM/dT)_1$ (emu/cm^3 K)	T_1(K)	ΔT_1(K)	$(dM/dT)_2$ (emu/cm^3 K)	T_2(K)	ΔT_2(K)
Heating (1 T)	49.5±7.8	348.2±0.5	10.1±0.6	44.3±9.3	358.8±0.5	9.6±0.6
Cooling (1 T)	53.1±4.6	338.0±0.3	11.9±0.5	84.6±9.6	344.4±0.1	3.50±0.2
Cycle H	$(dM/dH)_1$ (emu/cm^3 T)	$H_1(T)$	$\Delta H_1(T)$	$(dM/dH)_2$ (emu/cm^3 T)	$H_2(T)$	$\Delta H_2(T)$
Increasing field (340 K)	360.7±55.5	1.67±0.04	1.01±0.04	423.6±58.4	2.89±0.05	1.35±0.06
Decreasing field (340 K)	431.7±165.9	0.71±0.03	0.50±0.09	808.7±90.3	1.48±0.02	0.64±0.04

$$z_i = (H - H_i)/\Delta H_i. \tag{9}$$

The dM/dT profiles are almost identical to the dM/dH profiles for both systems, FeRh/MgO and FeRh/Al_2O_3, which underline that magnetic field and temperature have similar effects on the phase transition as can be expected from the linear temperature-field relationship shown previously for FeRh/MgO (Fig. 5). The fitting parameters used for the plots in Figs. 8(c) and 8(d) are summarized in Table II. We identify the peaks of the low and high temperature (field) Gauss function upon heating (increasing field) with the temperature (field) associated with the maximum nucleation and propagation rate of the F domains, respectively. Accordingly, the peaks of the high and low temperature (field) Gauss function upon cooling (decreasing field) can be identified with the temperature (field) associated with the maximum nucleation and propagation rate of the AF domains, respectively

Large thermal smearing of the first order phase transition of FeRh on MgO is observed, similar to that of Ru-doped $CeFe_2$ alloys (Refs. 15,16). This behavior generally is caused by inhomogeneities on some length scale, l, that will minimize the free energy of the system. While l has to be about the same as the correlation length, ξ, to influence the properties of an Ising type spin system, it needs to be much greater than ξ for an XY or Heisenberg type spin system, giving rise to domain formation.[23] Obviously the energy required for the creation of local domain walls has to be small compared to the energy required for a global transition. So the observed heterogeneous behavior implies that $l > \xi$.

Both the heating and cooling cycle of FeRh on MgO are identical, but are asymmetric in that the low temperature side is steeper than the high temperature side. A sharp AF nucleation peak as in the FeRh on sapphire sample is not observed. This means that nucleation of both F and AF domains seems to be heterogeneous and starts from the grain boundaries which makes an abrupt phase change impossible. According to the foregoing argument the domain nucleation in Ru-doped $CeFe_2$ also appears to be heterogeneous as well. The following is speculation but may motivate why the profile is asymmetric: What is measured experimentally is magnetization, not the fraction of volume that transitions into the F state. Initially F domains start to grow but are still below a critical size where long range order is established—consequently they are separated by regions of AF domains that may pin the magnetization of the F domains in a direction away from the magnetic field. Once the F domains grow to a critical size above which long range order is established they become unpinned from the vanishing AF domains and the magnetization will grow at an accelerated rate as it will start to orient towards the field direction.

In contrast to the FeRh on MgO sample which exhibits similar dM/dT profiles for heating and cooling, the AF nucleation peak for FeRh/Al_2O_3 is sharp compared to the F nucleation peak. This indicates that the initial transition into the AF state is much more homogeneous, which implies that $l < \xi$. In contrast, the transition into the F state seems heterogeneous as for FeRh/MgO. This asymmetry is similar to what is observed during the water to ice phase transition. An abrupt transition of water to ice can be observed in clean systems as the nucleation of ice crystals is homogeneous. In contrast, melting of ice is heterogeneous as it starts from the surface. Following this analogy we infer that the nucleation of F domains starts at the interface or grain boundaries of the FeRh film while nucleation of the AF domains starts homogeneously throughout the grains. While in water it is the surface tension that is responsible for the temperature hysteresis effect, in FeRh it appears to be the F-AF domain wall and strain energy.

VI. MEAN FIELD CALCULATION

To describe the first order phase transition in the FeRh film more quantitatively we follow the approach of Gruner *et al.*[26] and use a spin-1 Ising type model Hamiltonian also known as the Blume-Capel Hamiltonian,[27,28] which is used to describe Ising systems with first order phase transitions. In this Hamiltonian the spins can take the values +1,0,−1:

$$\mathsf{H} = -\sum_i D_i \vec{S}_i^2 - \sum_{\langle nn,nnn\rangle} J_{ik}\vec{S}_i\vec{S}_k - \vec{H}\sum_i \vec{S}_i\mu_i. \tag{10}$$

Although any real system would be more accurately described by a Heisenberg Hamiltonian the simplicity of an Ising model and its ability to produce qualitative results, such as the phase transition temperature shift upon applying an external field, is quite appealing. Moreover an Ising model seems justified in the case of FeRh since both the AF and the F phase exhibit a collinear spin- structure. The first term in Eq. (10) separates the nonmagnetic $S_i=0$ and mag-

netic $S_i=\pm 1$ states. D_{Fe} is on the order of several k_BT and positive to suppress the $S_i=0$ state for Fe atoms, D_{Rh} is negative to obtain nonmagnetic Rh atoms in the ground state. The second term is the Fe-Rh nearest and Fe-Fe next nearest neighbor exchange interaction. The sum runs over all Fe-Rh nearest neighbor and all Fe-Fe next nearest neighbor pairs. The Fe-Fe interaction J_{FeFe} is chosen to be negative to realize the AF ground state. The Fe-Rh interaction J_{FeRh} is positive and its magnitude larger than the Fe-Fe interaction to obtain the ferromagnetic phase. The Rh-Rh interaction is neglected. The last term is the Zeeman energy which contributes only to the F state and where H is the applied field, $\mu_{Fe}=3.2\ \mu_B$ for Fe and $\mu_{Rh}=0.9\ \mu_B$ for Rh, $\mu_B=5.79\times 10^{-5}$eV/T being the Bohr magneton.

While Gruner *et al.* used Monte Carlo simulations here we use a mean field approximation approach to qualitatively describe our observations. Note that this approach does not allow the reproduction of the temperature hysteresis, since a distribution of interaction energies and the creation of possible domain walls are neglected. Accordingly the spin-system will switch from the AF to the F state and vice versa in unison.

J_{FeFe} is fixed by the Néel temperature T_N of the AF phase assuming that no transition to the F phase takes place. T_N can be estimated as 620 K from the pressure-temperature phase diagram by extrapolating the transition line between AF and paramagnetic phase occurring at 6 GPa to zero pressure.[29] J_{FeRh} is determined by the Curie temperature $T_C=670$ K of the ferromagnetic phase.

For the AF phase only the Fe-Fe interactions need to be considered. The average z-component of the Fe spins is therefore

$$\langle S_{Fe}\rangle = B_1\left(\frac{q_{Fe}J_{FeFe}\langle S_{Fe}\rangle}{k_BT}\right). \tag{11}$$

For the F phase a coupled set of equations for the Fe and Rh spins needs to be considered. The average z component for Fe spins is

$$\langle S_{Fe}\rangle = B_1\left(\frac{q_{Fe}J_{FeFe}\langle S_{Fe}\rangle + q_{Rh}J_{FeRh}\langle S_{Rh}\rangle + \mu_{Fe}H}{k_BT}\right) \tag{12}$$

and the z component for the Rh spins is

$$\langle S_{Rh}\rangle = B_1\left(\frac{q_{Rh}J_{FeRh}\langle S_{Rh}\rangle + \mu_{Rh}H}{k_BT}\right) \tag{13}$$

where k_B is the Boltzman constant (8.62×10^{-5} eV/K), $q_{Rh}=8$ is the number of Fe-Rh nearest neighbor atoms, and $q_{Fe}=6$ is the number of Fe-Fe next nearest neighbor atoms, H is the applied field, $\langle S_{Fe}\rangle$ and $\langle S_{Rh}\rangle$ are the z components of the Fe and Rh spin operators, respectively. $B_n(x)$ denotes the nth Brillouin function

$$B_n(x) = \frac{2n+1}{2n}\coth\left(\frac{2n+1}{2n}x\right) - \frac{1}{2n}\coth\left(\frac{x}{2n}\right). \tag{14}$$

The magnetic moment is obtained by multiplying the spin values with 3.2 μ_B for Fe and 0.9 μ_B for Rh in the F phase and 3.3 μ_B in the AF phase. The change of the Fe and Rh moments in the AF and F phase is shown in Fig. 9. Clearly our choice of the exchange parameters J_{FeFe} and J_{FeRh} reproduce both a Néel temperature of 620 K and a Curie temperature of 670 K.

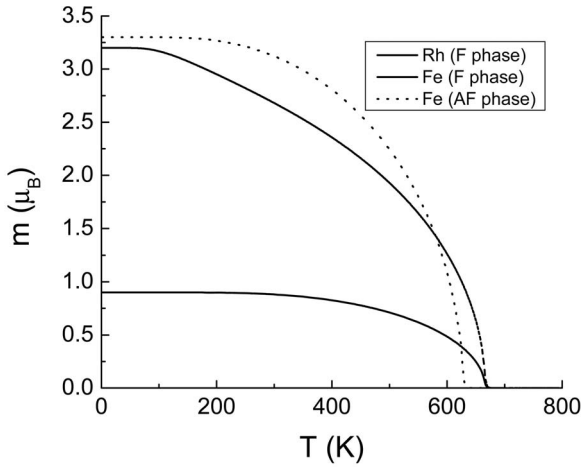

FIG. 9. Temperature dependence of the magnetic moment for the Fe and Rh atoms in the F and AF phases calculated within a mean field approach using a Blume-Capel Hamiltonian.

Since the observed temperature hysteresis effects are neglected the transition temperature from AF to the F phase is determined from the point where the free energy of the AF and F phases are equal, i.e., the free energy crossover point. The free energy is derived by

$$F(H,T) = E(H,T) - TS(H,T) = E(H,T) - T\int_0^T \frac{1}{T'}\frac{\partial E(H,T')}{\partial T'}dT', \tag{15}$$

where E is the inner energy derived from Eq. (10). The transition temperature of $T_M=360$ K can be attained by the correct choice of $D_{Rh}=-0.044$ eV.

The parameters used in the present calculation and those by Gruner *et al.* are summarized in units of electron-volts in Table III. Although J_{FeFe} is identical for both calculations, J_{FeRh} and D_{Rh} are significantly different. J_{FeRh} is off by approximately a factor of 2, which however may be founded in how the sum of Eq. (10) is evaluated.

The free energy per FeRh unit cell of the AF phase and the F phase with and without a 1 T applied field is shown in Fig. 10. When a magnetic field of 1 T is applied the transition temperature decreases −10 K to 350 K, which, considering the simplicity of our calculation, is in excellent agreement with the experimentally observed shifts of −8 K and to

TABLE III. Parameters in electron-volts for the spin-1 Ising model Hamiltonian [Eq. (10)].

	D_{Rh}	J_{FeRh}	J_{FeFe}	J_{RhRh}
This work (mean field)	−0.044	0.0150	−0.0135	0
Ref. 26 (Monte Carlo)	−0.151	0.0290	−0.0136	0

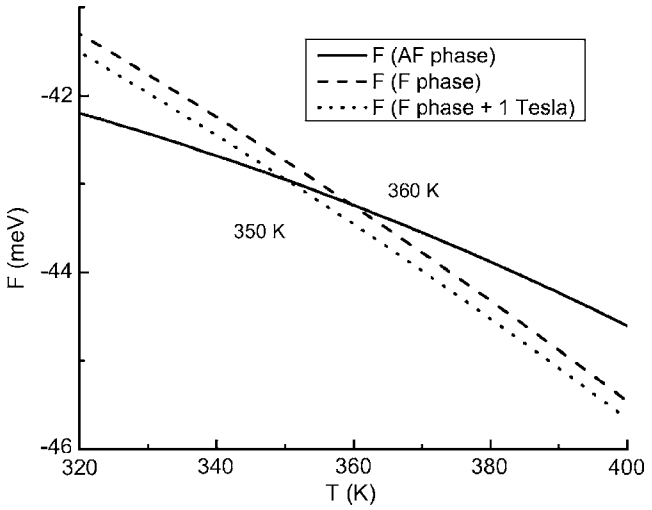

FIG. 10. Free energy per FeRh unit cell of the AF phase and the *F* phase with and without a 1 T external magnetic field. The calculated -10 K decrease of the transition temperature in a field of 1 T is in good agreement with the experimentally observed shift of −8 to −9 K for FeRh/MgO and FeRh/Al_2O_3, respectively. Model parameters are given in Table III.

−9 K for FeRh/MgO and FeRh on Al_2O_3, respectively. It can further be seen that the free energies of the *F* and AF phases vary about linearly in the temperature of interest and, hence, linear shifts with field can be expected. Thus, with our parameters we are able to accurately model not only the Curie and Néel temperature of the system, but also the transition temperature and its dependence upon applying an external field.

Neglecting the 1–2% lattice expansion accompanying the AF to *F* transition the entropy change at the transition can be calculated from Eq. (15) recognizing that the free energy for the AF and *F* phase is identical at the transition, which yields $\Delta S = 4.4 \times 10^5$ erg/cm^3=44 mJ/cm^3. This is about a factor of 3 smaller than what is observed. The difference between calculated and observed entropy values probably originates from neglecting the interaction of the electronic system with the lattice.

VII. SUMMARY

In summary the temperature and field hysteresis of the magnetization in the first order antiferromagnetic to ferromagnetic phase transition in FeRh films grown onto *c*-axis sapphire and MgO (001) was investigated. The FeRh film grown onto *c*-axis sapphire exhibits a lower transition temperature than the FeRh film grown onto MgO since tensile in-plane strain favors the ferromagnetic over the antiferromagnetic state. The transition to the ferromagnetic state upon heating and antiferromagnetic state upon cooling is generally broad indicating a heterogeneous transition induced defects. As a consequence, antiferromagnetic and ferromagnetic domains coexist during the transition. However, the nucleation of antiferromagnetic domains upon cooling is abrupt for FeRh on *c*-axis sapphire which is indicative of homogeneous nucleation and growth of AF domains.

The transition is further broadened when measuring with fields applied out of plane of the sample due to internal demagnetization fields. Applying an external magnetic field generally stabilizes the ferromagnetic phase and consequently decreases the transition temperature. Temperature dependent remanent magnetization measurements reveal that field induced magnetization changes are irreversible during heating, but reversible during cooling. The field dependence of the shift in transition temperature is qualitatively modeled with an Ising spin type model utilizing a mean field approach. From this calculation a shift of −10 K/T in transition temperature is determined which compares well with the experimentally observed shift of −8 and −9 K/T for FeRh films grown onto MgO (001) and c-axis sapphire, respectively.

ACKNOWLEDGMENT

We feel indebted to Andrew Kellock at IBM for performing the Rutherford backscattering experiments.

[1] M. Fallot, Ann. Phys. **10**, 291 (1938).
[2] M. Fallot and R. Horcart, Rev. Sci. **77**, 498 (1939).
[3] A. I. Zakharov, A. M. Kadomtseva, R. Z. Levitin, and E. G. Ponyatovskii, Zh. Eksp. Teor. Fiz. **46**, 2003 (1964) [Sov. Phys. JETP **19**, 1348 (1964)].
[4] L. Zsoldos, Phys. Status Solidi **20**, K25 (1967).
[5] J.-U. Thiele, S. Maat, Eric E. Fullerton, and J. L. Robertson, IEEE Trans. Magn. **40**, 2537 (2004).
[6] M. R. Ibarra and P. A. Algarabel, Phys. Rev. B **50**, 4196 (1994).
[7] J. S. Kouvel and C. C. Hartelius, J. Appl. Phys **33**, 1343 (1962).
[8] N. V. Baranov and E. A. Baranove, J. Alloys Compd. **219**, 139 (1995).
[9] M. P. Annaorazov, S. A. Nikitin, A. L. Tyurin, K. A. Asatryan, and A. Kh. Dovtetov, J. Appl. Phys. **79**, 1689 (1996).
[10] J. S. Kouvel, J. Appl. Phys. **37**, 1257 (1966).
[11] J. M. Lommel, J. Appl. Phys. **40**, 3880 (1969).
[12] P. Tu, A. J. Heeger, J. S. Kouvel, and J. B. Comly, J. Appl. Phys. **40**, 1368 (1969).
[13] P. H. L. Walter, J. Appl. Phys. **33**, 938 (1964).
[14] G. Shirane, C. W. Chen, P. A. Flinn, and R. Nathans, J. Appl. Phys. **34**, 1044 (1963).
[15] G. Shirane, C. W. Chen, and R. Nathans, Phys. Rev. **134**, A1547 (1964).
[16] M. K. Chattopadhyay, S. B. Roy, A. K. Nigam, K. J. S. Sokhey, and P. Chaddah, Phys. Rev. B **68**, 174404 (2003).
[17] S. B. Roy, G. K. Perkins, M. K. Chattopadhyay, A. K. Nigam, K. J. S. Sokhey, P. Chaddah, A. D. Caplin, and L. F. Cohen, Phys. Rev. Lett. **92**, 147203 (2004).
[18] J.-U. Thiele, S. Maat, and E. E. Fullerton, Appl. Phys. Lett. **82**, 2859 (2003).

[19] K. Y. Guslienko, O. Chubykalo-Fesenko, O. Mryasov, R. Chantrell, and D. Weller, Phys. Rev. B **70**, 104405 (2004).
[20] J.-U. Thiele, M. Buess, and C. H. Back, Appl. Phys. Lett. **85**, 2857 (2004).
[21] G. Ju, J. Hohlfeld, B. Bergman, R. J. M. Van de Veerdonk, O. N. Mryasov, J. Y Kim, X. Wu, D. Weller, and B. Koopmans, Phys. Rev. Lett. **93**, 192301 (2004).
[22] S. Chikazumi, *Physics of Ferromagnetism*, 2nd ed. (Clarendon Press, Oxford, 1997), p. 120.
[23] Y. Imry and M. Wortis, Phys. Rev. B **19**, 3580 (1979).
[24] R. E. Camley, W. Lohstroh, G. P. Felcher, N. Hosoito, and H. Hashizume, J. Magn. Magn. Mater. **286**, 65 (2005).
[25] J. B. McKinnon, D. Melville, and E. W. Lee, J. Phys. C **1**, S46 (1970).
[26] M. E. Gruner, E. Hoffmann, and P. Entel, Phys. Rev. B **67**, 064415 (2003).
[27] M. Blume, Phys. Rev. **141**, 517 (1966).
[28] H. W. Capel, Physica (Amsterdam) **32**, 966 (1966).
[29] R. C. Wayne, Phys. Rev. **170**, 523 (1968).